Available on CMS information server

CMS AN 2009/XXX

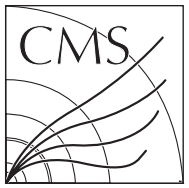

The Compact Muon Solenoid Experiment

Analysis Note

The content of this note is intended for CMS internal use and distribution only

November 7, 2009 **DRAFT**

Particle Flow Jet Composition

Francesco Pandolfi, Daniele del Re

"Sapienza" Università di Roma e Sezione dell'INFN, Roma, Italy

Mikko Voutilainen

CERN, European Organization for Nuclear Research, Geneva, Switzerland

Abstract

A study of the Particle Flow jet energy composition is presented. It proves to be a crucial aspect to be monitored on first LHC data, because Particle Flow jet reconstruction performance heavily depends on its particle composition. The charged hadron component, furthermore, proves to be a valid meter of the quality with which the jet has been measured.

Contents

1 Introduction

The Particle Flow event reconstruction [1] aims at giving a complete description of the event by reconstructing all final state stable particles. In order to do this, all CMS sub-detectors are exploited in unison in an optimal way. Reconstructed particle candidates are then grouped together to form Particle Flow jets.

The Particle Flow approach substantially improves jet reconstruction in CMS, delivering jets that are measured more accurately than the ones provided by calorimeter-based reconstruction algorithms. This phenomenon is amplified at low p_{T}, and is due to three main reasons:

- the Particle Flow algorithm is constructed in such a way that at low p_{T} it makes more extensive relying on the very precise track information; calorimeter jets, conversely, are very inaccurate at low energies, with their resolution dominated by the fluctuations induced by the noise and stochastic HCAL terms;
- soft charged jet particles are bent away by the 3.8 T magnetic field, and therefore create deposits far away in the calorimeter with respect to the jet axis; these particles can be recovered by making use of the tracker information, whereas in a calorimeter stand-alone approach they are invariably lost;
- the superior tracker granularity allows a correct inter-particle momentum subdivision even for collimated bunches of particles, resulting in a more accurate evaluation of the jet 4-vector.

Compared to traditional jet reconstruction, though, a Particle Flow jet is a more complex object. Therefore, more detailed analyses can and must be done in order to monitor and improve their performance.

This note describes one of such methods, based on the study of a Particle Flow jet's particle composition. Different

Table 1: Analyzed 'Summer 09' QCD di-jet samples. For each sample, its DBS instance, cross section (σ), and number of events is given.

DBS Instance	σ **[pb]**	**Events**
/QCDDiJetPt0to15/Summer09-MC_31X_V3-v1/GEN-SIM-RECO	$5.16 \cdot 10^{10}$	2516828
/QCDDiJetPt15to20/Summer09-MC_31X_V3-v1/GEN-SIM-RECO	$9.49 \cdot 10^{8}$	2018990
/QCDDiJetPt20to30/Summer09-MC_31X_V3-v1/GEN-SIM-RECO	$4.01 \cdot 10^{8}$	1696590
/QCDDiJetPt30to50/Summer09-MC_31X_V3-v1/GEN-SIM-RECO	$9.47 \cdot 10^{7}$	1094811
/QCDDiJetPt50to80/Summer09-MC_31X_V3-v1/GEN-SIM-RECO	$1.22 \cdot 10^{7}$	119642
/QCDDiJetPt80to120/Summer09-MC_31X_V3-v1/GEN-SIM-RECO	$1.62 \cdot 10^{6}$	551544
/QCDDiJetPt120to170/Summer09-MC_31X_V3-v1/GEN-SIM-RECO	$2.56 \cdot 10^{5}$	54568
/QCDDiJetPt170to230/Summer09-MC_31X_V3-v1/GEN-SIM-RECO	$4.83 \cdot 10^{4}$	55000
/QCDDiJetPt230to300/Summer09-MC_31X_V3-v1/GEN-SIM-RECO	$1.06 \cdot 10^{4}$	54028
/QCDDiJetPt300to380/Summer09-MC_31X_V3-v1/GEN-SIM-RECO	$2.63 \cdot 10^{3}$	52356
/QCDDiJetPt380to470/Summer09-MC_31X_V3-v1/GEN-SIM-RECO	$7.22 \cdot 10^{2}$	54559
/QCDDiJetPt470to600/Summer09-MC_31X_V3-v1/GEN-SIM-RECO	$2.41 \cdot 10^{2}$	55905
/QCDDiJetPt600to800/Summer09-MC_31X_V3-v1/GEN-SIM-RECO	$6.25 \cdot 10^{1}$	21424
/QCDDiJetPt800to1000/Summer09-MC_31X_V3-v1/GEN-SIM-RECO	9.42	21028
/QCDDiJetPt1000to1400/Summer09-MC_31X_V3-v1/GEN-SIM-RECO	2.34	21784
/QCDDiJetPt1400to1800/Summer09-MC_31X_V3-v1/GEN-SIM-RECO	$1.57 \cdot 10^{-1}$	21810
/QCDDiJetPt1800to2200/Summer09-MC_31X_V3-v1/GEN-SIM-RECO	$1.38 \cdot 10^{-2}$	21730
/QCDDiJetPt2200to2600/Summer09-MC_31X_V3-v1/GEN-SIM-RECO	$1.30 \cdot 10^{-3}$	22013
/QCDDiJetPt2600to3000/Summer09-MC_31X_V3-v1/GEN-SIM-RECO	$1.14 \cdot 10^{-4}$	22046
/QCDDiJetPt3000to3500/Summer09-MC_31X_V3-v1/GEN-SIM-RECO	$8.43 \cdot 10^{-6}$	20908
/QCDDiJetPt3500toInf/Summer09-MC_31X_V3-v1/GEN-SIM-RECO	$1.81 \cdot 10^{-7}$	21060

Table 2: Analyzed 'Summer 09' Photon+Jet samples. For each sample, its DBS instance, cross section (σ), and number of events is given.

DBS Instance	σ **[pb]**	**Events**
/PhotonJetPt15/Summer09-MC_31X_V3-v1/GEN-SIM-RECO	$2.89 \cdot 10^5$	1073270
/PhotonJetPt30/Summer09-MC_31X_V3-v1/GEN-SIM-RECO	$3.22 \cdot 10^4$	1006118
/PhotonJetPt80/Summer09-MC_31X_V3-v1/GEN-SIM-RECO	$1.01 \cdot 10^3$	1003673
/PhotonJetPt170/Summer09-MC_31X_V3-v1/GEN-SIM-RECO	51.4	1496900
/PhotonJetPt300/Summer09-MC_31X_V3-v1/GEN-SIM-RECO	4.19	1048016
/PhotonJetPt470/Summer09-MC_31X_V3-v1/GEN-SIM-RECO	0.45	1014413
/PhotonJetPt800/Summer09-MC_31X_V3-v1/GEN-SIM-RECO	0.02	1241880
/PhotonJetPt1400/Summer09-MC_31X_V3-v1/GEN-SIM-RECO	$2.68 \cdot 10^{-4}$	1012410

jet sub-populations can be defined, depending on what fraction of its energy is carried by a certain type of particles. Studying the jet qualities as a function of the variations of these energy fractions gives powerful insight on the nature of the jet itself. One of these variables, the fraction of jet energy carried by charged hadron candidates, proves to be a valid meter of the quality with which the jet has been reconstructed. It can therefore be exploited at analysis level, to select Particle Flow jets that have been measured more accurately, or as a calibration variable, to optimally take into account different classes of jet sub-populations.

2 Data Samples

This analysis makes use of two different sets of data samples from the 'Summer 09' production. These events have all been generated and reconstructed with the `CMSSW_3_1_X` software release series, at a centre of mass energy $\sqrt{s} = 10$ TeV. The analysis has been made entirely in `CMSSW_3_1_2`.

The results presented in Sections 4 and 5 have been obtained by analyzing the QCD di-jet samples, which have been generated in 21 parton transverse momentum ($\hat{p}_\mathrm{T}$) bins. The DBS instances of these datasets, as well as the corresponding cross sections and number of events, are shown in Table 1. On the other hand, the data-driven method for computing and applying such corrections, described in Section **??**, makes use of the Photon+Jet samples, listed in Table 2. These events have instead been generated in open $\hat{p}_\mathrm{T}$ intervals, comprising of events with $\hat{p}_\mathrm{T}$ greater than a certain threshold.

All events have been correctly weighted on the relative cross sections. In order to do so, a cut on $\hat{p}_\mathrm{T}$ has been applied to the Photon+Jet events, to eliminate overlapping values of $\hat{p}_\mathrm{T}$ between different datasets.

3 Definitions

Particle jets are defined by choosing a proper jet clustering algorithm. The analysis presented in this note consideres only jets clustered with the anti-k_T algorithm [2], with size parameter $R = 0.5$. The same algorithm is applied to generated MC truth particles, obtaining generated jets, and to PFCandidates, obtaining reconstructed Particle Flow jets (see Section 4 for details). To access the Monte Carlo truth information, reconstructed jets are subsequently matched to generated jets by requiring

$$\Delta R \equiv \sqrt{\Delta\eta^2 + \Delta\phi^2} < 0.1$$

where $\Delta\eta$ and $\Delta\phi$ are respectively the differences in pseudorapidity and azimuth between the reconstructed and the generated jets. In the case of multiple generated jets satisfying this condition, the closest one is selected.

The two main variables used in the study of jet reconstruction performance are the energy response and energy resolution. The energy response, in a given p_T bin, is usually defined as the mean of the

$$p_\mathrm{T}^\mathrm{RECO}/p_\mathrm{T}^\mathrm{GEN}$$

distribution, where $p_\mathrm{T}^\mathrm{RECO}$ is the reconstructed jet's transverse momentum, and $p_\mathrm{T}^\mathrm{GEN}$ is the generated jet's one. The energy resolution is then defined as the standard deviation of such distribution, divided by the response. From now on we will refer to response and resolution computed in this way as "arithmetic".

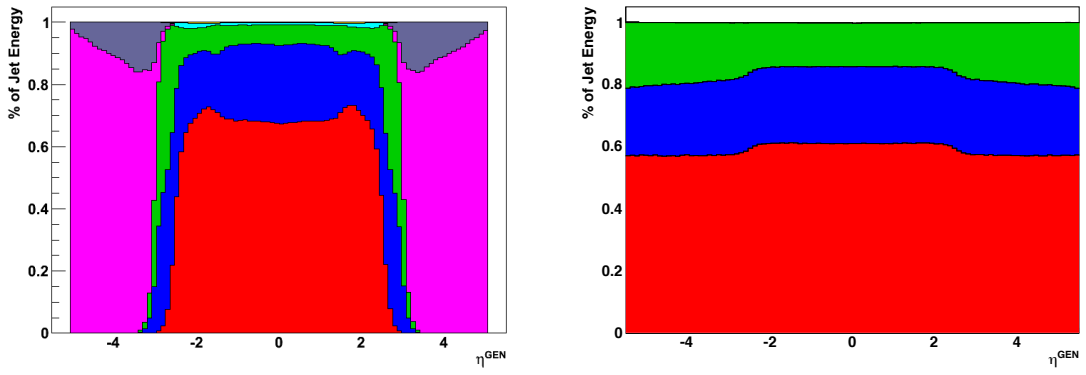

(a) (b)

Figure 1: Average jet energy compisition as a function of generated pseudorapidity η^{GEN} for PFJets (a) and generated jets (b). From bottom to top: charged hadrons (red), photons (blue) and neutral hadrons (green), electrons (cyan). Furthermore, in the reconstructed spectrum, particles in the $3 < |\eta| < 5$ region are detected by HF and identified as hadrons (magenta) or electromagnetic particles (grey, on top). See text for details.

For the purpose of this note, however, we will also obtain these two quantities from a gaussian fit to the distributions. The fit function will be initialized with mean and width equal respectively to the mean and RMS of the distribution, and the fit will be extended in an interval of ± 2 standard deviations about the mean, in a 3-step iterative procedure. The response will then be obtained as the resulting function's mean parameter, while the energy resolution as the width divided by the response. The method used for the extraction of the jet energy response and resolution, be it arithmetic or from a fit, will nevertheless always be specified.

4 Jet Particle Composition

The aim of the Particle Flow reconstruction strategy is to provide a complete description of an event by identifying all stable particles. The algorithm therefore analyzes all of the reconstructed "elements" in an event (i.e. tracks, ECAL clusters, HCAL deposits, etc.) to create particle candidates. The algorithmic procedure through which Particle Flow particle candidates (in short PFCandidates) are created is rather complex, for it makes use of ingenious strategies in order to avoid multiple counting of reconstructed energy. It is thoroughly described in [1].

For what concernes the scope of this note, it is sufficient to say that PFCandidates can be of seven different types, depending on the subdetectors that were used in their reconstruction:

1. Charged Hadron
2. Electron
3. Muon
4. Photon
5. Neutral Hadron
6. HF Hadronic Particle
7. HF EM Particle

We must point out, though, that while the creation of PFCandidates is quite straightforward in the case of isolated particles (a Particle Flow photon is created from an ECAL cluster that is not "linked" to tracks or HCAL deposits, a Particle Flow muon when compatible hits are found in the inner tracking system and the muon chambers, and so forth), some complexities arise with bunched particles, such as the case of jets. This is because, while the CMS tracker is able to distinguish charged particles with high efficiency and excellent granularity, neutral particle detection is based on the energy deposits seen in the calorimeters, and is therefore heavily dependant on their resolutions and granularities. While this is not much of a concern for CMS's superb electromagnetic calorimeter, HCAL's inferior performance may limit the reconstruction discrimination power.

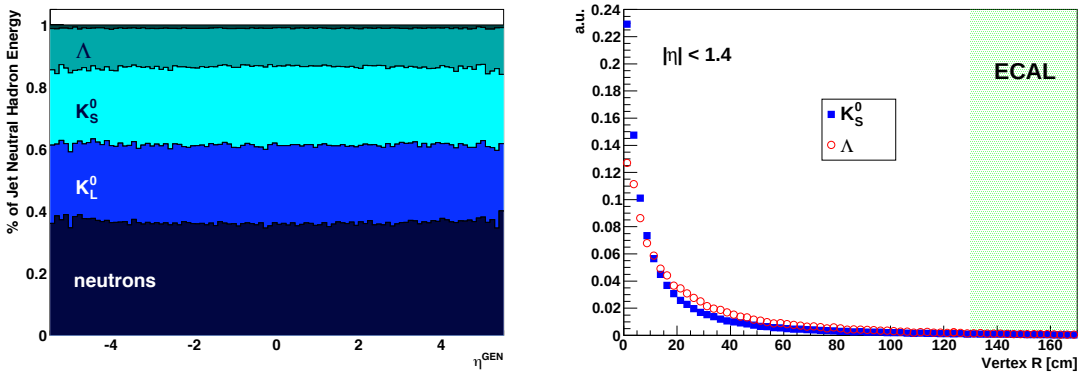

(a) (b)

Figure 2: (a): Generated jet neutral hadron energy composition, as a function of the jet pseudorapidity. From bottom to top, neutral hadron energy contributions from neutrons, K^0_L's, K^0_S's, Λ's, and, on top (but not labeled on the figure), Ξ^0's. (b): Distribution of the MC truth radial distance of the decay vertices for K^0_S (blue squares) and Λ (red circles) mesons produced in the barrel. The shaded band on the left shows the position of ECAL.

When a reconstructed track is found to point to a calorimeter energy deposit, the Particle Flow algorithm adopts the following strategy. The sum of the momenta of the tracks $\sum p_{\rm tracks}$ is computed, and it is compared to the sum of the interested calorimetric (ECAL and HCAL) clusters $E_{\rm calo}$. If these two quantities are compatible within one standard deviation of the expected HCAL energy resolution, a Particle Flow charged hadron is created for each track, under the pion mass hypothesis. If, on the other hand, a calorimetric energy excess $E_{\rm excess}$ is observed, two cases may arise: if the excess is smaller that the total ECAL clustered energy $E_{\rm ECAL}$, a Particle Flow photon is created to account for $E_{\rm excess}$; conversely, if $E_{\rm excess} > E_{\rm ECAL}$, both a Particle Flow photon with energy equal to $E_{\rm ECAL}$ and a Particle Flow neutral hadron with energy equal to $(E_{\rm excess} - E_{\rm ECAL})$ are created.

4.1 Energy Fraction Variables

With seven different PFCandidate types, we can introduce seven corresponding variables, that we will call respectively $\rm R_{ch}$, $\rm R_e$, $\rm R_\mu$, $\rm R_\gamma$, $\rm R_{nh}$, $\rm R_{HFhad}$ and $\rm R_{HFem}$, defined as

$$\rm R_X = \frac{\sum E_X}{E_{jet}}$$

where the sum is extended over all PFCandidates of type 'X' composing the considered jet, and $E_{\rm jet}$ is the total jet energy. These variables therefore represent the fraction of jet energy that is carried by 'X-type' PFCandidates.

The study of the average value of these variables as a function of pseudorapidity gives insight on the expected PFJet composition in the CMS detector. This is shown in Figure 1a, for PFJets correctly matched to generated jets, as a function of the matched generated jet's pseudorapidity ($\eta_{\rm GEN}$). Furthermore, a cut on the generated transverse momentum has been applied ($p_{\rm T}^{\rm GEN} > 80$ GeV/c). As expected, the charged energy fraction $\rm R_{ch}$ starts dropping

Table 3: Principal decay modes and branching ratios (BR) for short-lived neutral hadrons. Values are taken from [3].

Particle	Decay Channel	BR
K^0_S	$\pi^+\pi^-$	69.2%
	$\pi^0\pi^0$	30.7%
Λ	$p\,\pi^-$	63.9%
	$n\,\pi^0$	35.8%
Ξ^0	$\Lambda\,\pi^0$	99.5%

in correspondance of $|\eta_{\rm GEN}| = 2.5$, where the silicon tracker ends. Similarly, central calorimetry reaches up to $\eta = 3$, which is where the photon and neutral hadron components start giving way to the HF components.

An equivalent jet composition spectrum can be constructed for generated jets (Figure 1b), by discriminating on the generated particles that compose these jets. In this case, though, a little delicacy is required. In fact, while classification of particles such as prompt photons and charged hadrons is quite straightforward, some complications arise in the case of neutral hadrons, for these should be classified on the basis of the actual detector reconstruction capabilities.

The average generated jet neutral hadron composition, as a function of jet pseudorapidity, is shown in Figure 2a. About 60% of these particles are neutrons and K_L^0, which have long enough lifetimes to ensure that they reach the calorimeters without decaying. On the other hand, the remaining 40% is composed of relatively short lived particles, which decay before reaching the calorimeters. The dominant decay channels for these particles are shown in Table 3, while Figure 2b shows the distribution of the radial distance of the MC truth decay vertices for particles produced in the barrel ($|\eta_{\rm GEN}| < 1.4$).

Neutral hadrons that decay in the CMS tracker must be classified on the basis of their decay product. Neutral pions, in particular, will rapidly decay to photons and therefore be detected in the electromagnetic calorimeter. For this reason it is correct, in the ECAL-covered pseudorapidity region, to add their energy to the photon spectrum: this explains the rise in the photon component in Figure 1b, in correspondence of the $|\eta_{\rm GEN}| < 3$ region.

As for the decay to charged hadrons, the discimination is based on whether the decay vertex lies in a track seeded region of the detector or not. In the current version of the CMS software, the Particle Flow algorithm makes use of only four steps (out of five) of the CMS Iterative Tracking [4]. In this implementation, track finding is guaranteed to have good efficiency even for charged particles originating from displaced secondary vertices as far as a radius of $R \approx 30$ cm deep in the transverse plane. Consequently, charged hadrons produced at $R < 30$ cm will be placed in the charged hadron component, whereas hadrons produced deeper in the detector will be kept in the neutral hadron one. For this reason the charged fraction in Fig. 1b shows a discontinuity at $|\eta| = 2.5$.

The same method has been applied to photons in jets. If a photon converts to an electron-positron pair in a track seeded region of the detector, its energy will be accounted for in the electron energy fraction. Otherwise, in the photon one.

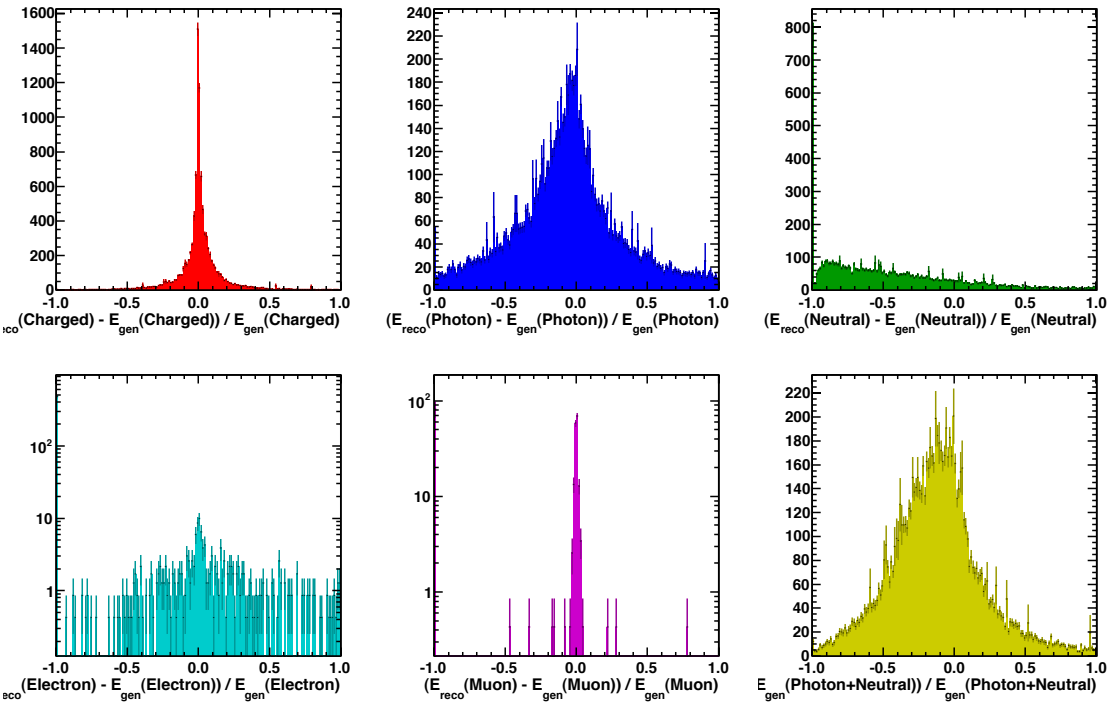

Figure 3: Single component energy resolutions for PFJets matched to generated jets with $87 < p_{\rm T} < 104$ GeV/c: charged hadron resolution (top left), photon resolution (center top), neutral hadron resolution (top right), electron resolution (bottom left), muon resolution (center bottom), photon+neutral hadron resolution (bottom right).

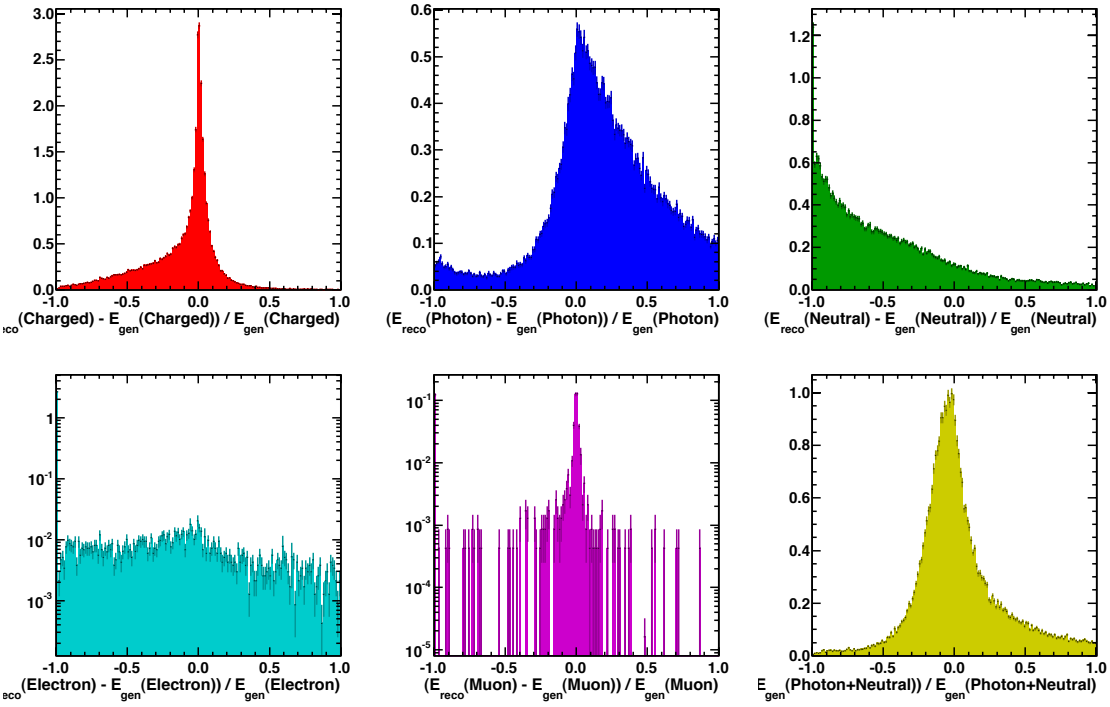

Figure 4: Single component energy resolutions for PFJets matched to generated jets with $523 < p_{\mathrm{T}} < 627$ GeV/c: charged hadron resolution (top left), photon resolution (center top), neutral hadron resolution (top right), electron resolution (bottom left), muon resolution (center bottom), photon+neutral hadron resolution (bottom right).

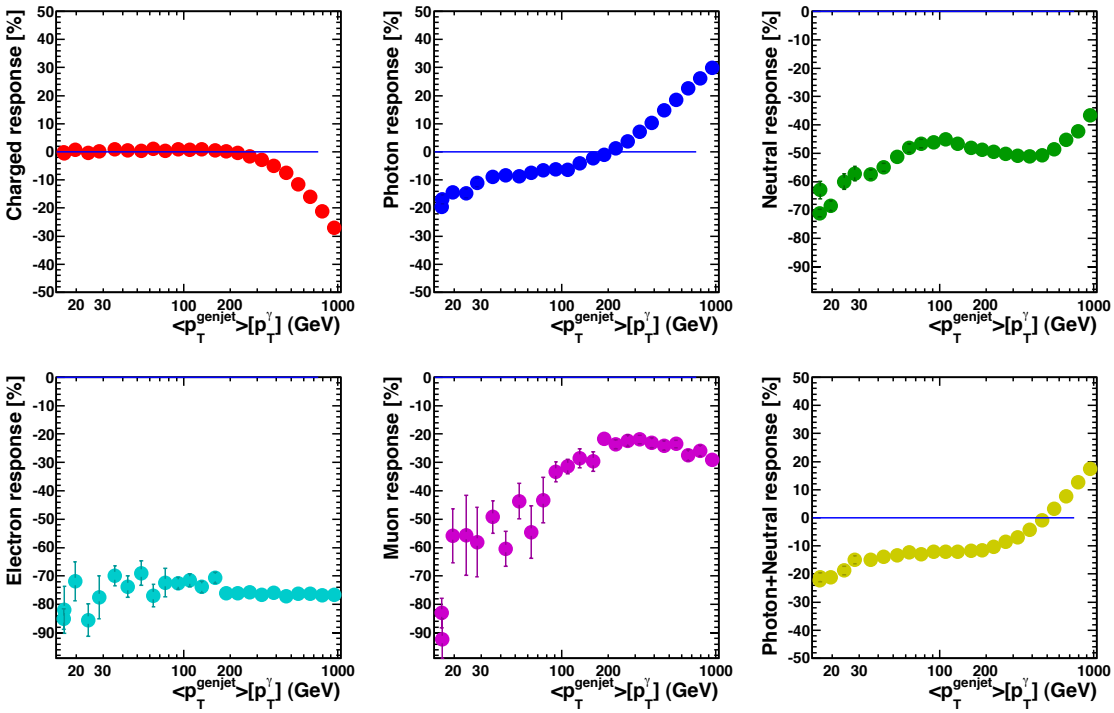

Figure 5: Single component energy response as a function of jet transverse momentum: charged hadron response (top left), photon response (center top), neutral hadron response (top right), electron response (bottom left), muon response (center bottom), photon+neutral hadron response (bottom right).

4.2 Single Component Resolutions

A component-based study of PFJets is both useful to obtain an in-depth understanding of the Particle Flow jet reconstruction, and an invaluable tool to monitor their behaviour on first data and test the accuracy of the CMS Monte Carlo simulation. As we will se more thoroughly in the next section, Particle Flow jet reconstruction performance depends dramatically on the considered jet's composition, so that a crucial step in Particle Flow validation on data will be to assure that a correct energy sharing between components is assigned during jet creation.

Figures 3 and 4 show, for two different p_{T} bins, single component energy resolutions for PFJets reconstructed in the CMS barrel. For a given component 'X', the resolution is defined as:

$$\frac{E_{\mathrm{X}}^{\mathrm{reco}} - E_{\mathrm{X}}^{\mathrm{gen}}}{E_{\mathrm{X}}^{\mathrm{gen}}}$$

with obvious meaning of the simbols. Figure 5, instead, shows the energy response for each component, computed as the mean of such resolution distributions, as a function of the jet transverse momentum.

As expected, the excellent performance of the CMS tracker translates in very sharp peak in the charged energy resolution. A somewhat broader distribution is obtained for the photon resolution, while for neutral hadrons an excessively large fraction of reconstructed jets (note the logarithmic scale of the y-axis) seem to report no neutral hadron presence, whereas the corresponding generated jets did (note the over-population of the '-1' bin).

Both the asymmetry in the photon spectrum and the anomalies in the neutral hadron one are consequence of the Particle Flow reconstruction strategy. In the case of jets, both photons and neutral hadrons, as previously described, are constructed only if a calorimetric energy excess is observed, with respect to the measured momenta of the tracks pointing to these energy deposit. Furthermore, when an excess is actually observed, precedence in always given to photon candidate creation. For these reasons it is more sound to study the *combined* photon and neutral hadron resolution, which is shown in the bottom right plots. The obtained distribution is strikingly more symmetric, but has an evident bias. The amount of the bias should be directly connected to the HCAL energy resolution, on which is based the comparison that eventually gives rise to photons and neutral hadrons in jets.

At jet transverse momenta greater than ≈ 500 GeV/c tracking charged collimated particles becomes a more and more difficult task, with a growing probability of 'loosing' particle tracks due to rec-hit sharing or similar effects. The charged energy component therefore increasingly underestimates the correct value, and this traslates into the formation of a visible tail on the left of the resolution distribution (see Figure 4). The Particle Flow algorithm, though, compensates this effect because the energy is measured in the calorimeter, and is therefore not lost. So even if this leads to a gradual underestimation of the charged component and a gradual overestimation of the combined neutral one, on the whole the jet measurement is more precise as its transverse momentum increases.

5 Response and Resolution Variation with Jet Charged Energy Fraction

If the advantage of PFJets over calorimeter jets relies in the access to the central tracker information, it is quite straightforward to parametrize it through the variable $\mathrm{R_{ch}}$. We expect to have jets of "higher quality" (i.e. higher reponse and better resolution) with increasing $\mathrm{R_{ch}}$, because of a more intense use of the tracker. Figures 6a,b show jet arithmetic response and resolution variations as a function of the generated jet's transverse momentum, in three $\mathrm{R_{ch}}$ intervals, for PFJets generated in the CMS barrel ($|\eta| < 1.4$). Figures 6a,b show the same variations for response and resolution obtained by gaussian fits to the distributions.

For transverse momenta up to a few hundred GeV$/c$, jet quality increases with $\mathrm{R_{ch}}$. The effect is particularly visible in the resolution graph, where at low-p_{T} the spread can be as large as 60%. At high-p_{T}, instead, the hierarchy is completely inversed: at large values of $\mathrm{R_{ch}}$, jet reconstruction quality drops visibly. This effect is caused by the increasing unreliability of tracking in the case of collimated, high-p_{T} particles, and has been already discussed in Section 4.2.

@@@ What is actually happening must be understood. feedback from the PF group is needed.

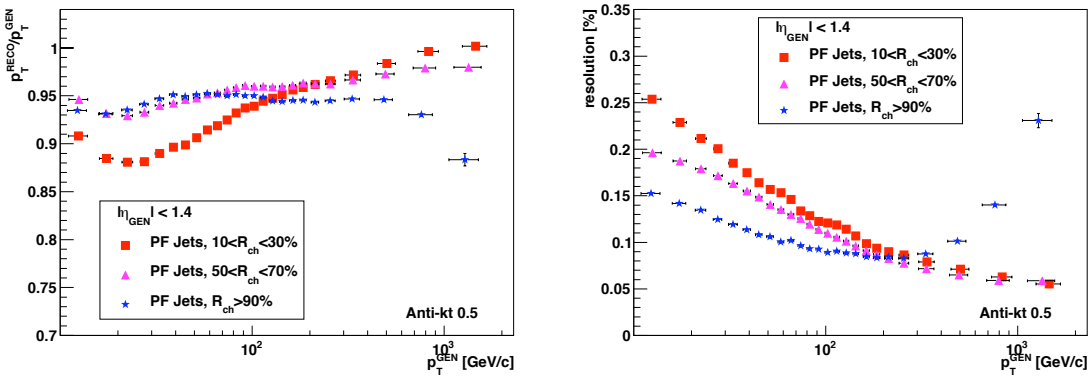

(a) (b)

Figure 6: PFJet energy arithmetic response (a) and resolution (b) for different R_{ch} intervals.

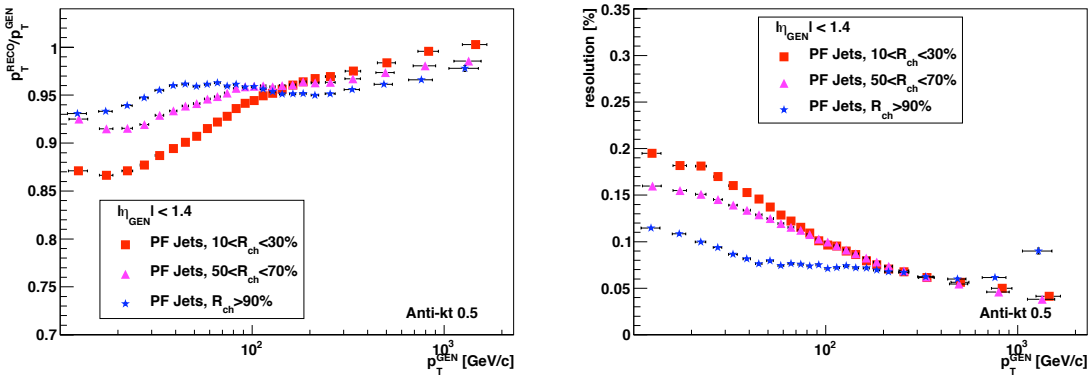

(a) (b)

Figure 7: PFJet energy response (a) and resolution (b) for different R_{ch} intervals. Response and resolution have been obtained through gaussian fits to the response distributions.

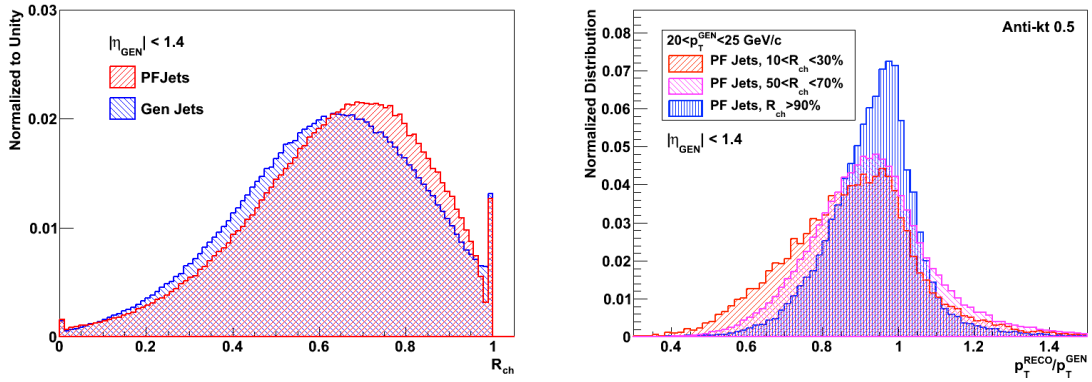

(a) (b)

Figure 8: (a): R_{ch} distributions for PFJets and generated jets in the CMS barrel, with $p_T^{GEN} > 80$ GeV/c; (b): jet response distributions for barrel PFJets with $20 < p_T^{GEN} < 25$ GeV/c.

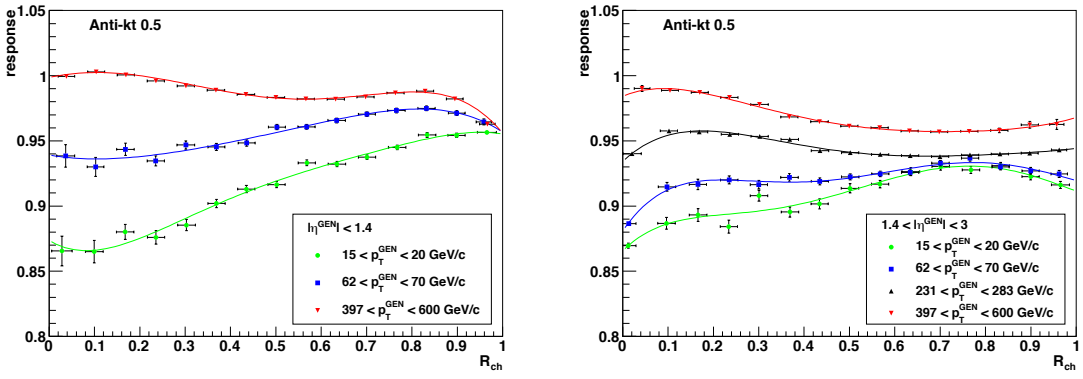

(a) (b)

Figure 9: MC truth jet energy response as a function of charged jet energy fraction R_{ch}, for different p_T bins, in the barrel (a) and in the endcaps (b). Data points are fitted with a fifth-order polinomial.

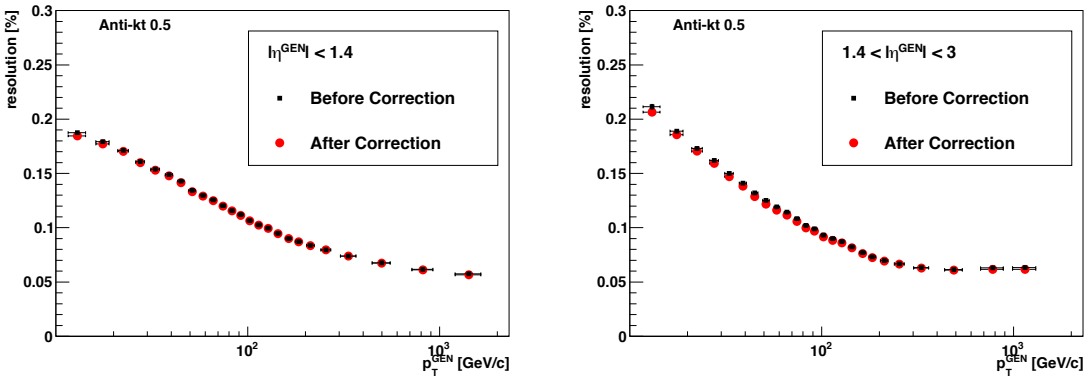

(a) (b)

Figure 10: MC truth jet arithmetic energy resolution as a function of generated jet transverse momentum in the barrel (a) and in the endcaps (b), before (black squares) and after (red circles) the application of the R_{ch}-based correction.

Figure 8a shows the reconstructed and generated R_{ch} distributions for barrel PFJets. A tranverse momentum cut of p_T has been applied on the generated jets. Figure 8b, instead, shows jet response distributions for jets with $20 < p_T < 25$ GeV/c, in the three studied R_{ch} intervals.

5.1 R_{ch}-Based Calibration

From what has been shown it is clear that the jet charged energy fraction R_{ch} is a valid meter of the quality with which the considered jet has been measured. For the simple reason that a jet that is measured more accurately requires less (or none) energy corrections with respect to a jet that is measured poorly, we will here make a Monte Carlo feasibility test to see if it possible to use R_{ch} as a calibration variable, to optimally exploit these different jet sub-populations.

In order to do so, the variation of the response as a function of R_{ch} will be studied for each p_T^{GEN} bin. The data points in each such bin are fitted with a fifth-order polinomial, and the correction is obtained as the inverse of the fitted response. Figures 9a and 9b show, respectively for barrel and endcaps, the obtained MC-truth variation for some p_T bins. The fit function is superimposed, and an overall good agreement is observed. The data points show that the response variation as a function of R_{ch} is more pronounced at low p_T, becomes almost negligible intermediate p_T and finally tends to invert monotony at high p_T. Furthermore, the observed variation in the endcaps is very little.

Figures 10a and 10b show the obtained MC-truth variation in PFJet arithmetic resolution, for barrel and endcaps, when applying the R_{ch}-based correction. The gain is mainly concentrated in the low-p_T end of the spectrum, and never greater than 0.5%. The variation is even smaller in the fit resolutions. Considering that the introduction of this method would imply a certain degree of uncertainty connected to the systematic effects intrinsic to the method,

we conclude that it is simply not worth it.

6 Conclusions

The study of the energy composition of Particle Flow jets proves to be an invaluable tool for the understanding and monitoring of both the Particle Flow algorithm as a whole and, more specifically, the Particle Flow jet reconstruction. Because particles are measured with very different precision depending on which subdetectors are used and what energy regime is considered, Particle Flow jet reconstruction performance heavily depends on the jet's composition. It will therefore be crucial to verify on the first LHC collision data that the Particle Flow algorithm is correctly describing particle jets in terms of energy components. This type of analysis will furthermore play an important role in tuning the Monte Carlo simulation of the experiment to match the observed data.

References

[1] **CMS** Collaboration, *Particle-Flow Event Reconstruction in CMS and Performance with Jets, Taus and* $E_{\mathrm{T}}^{\mathrm{miss}}$, CMS PAS PFT-09/001

[2] M. Cacciari, G. P. Salam and G. Soyez, *The anti-kt jet clustering algorithm*, JHEP 0804 (2008) 063 [arXiv:0802.1189]

[3] C. Amsler et al., *The Review of Particle Physics*, Physics Letters **B** 667 (2008)

[4] **CMS** Collaboration, *Track Reconstruction in the CMS tracker* (in preparation), CMS-PAS TRK-09-001 (2009)